



*Conference Proceedings of the 5th Asia Pacific Luminescence and Electron Spin Resonance Dating Conference
October 15th-17th, 2018, Beijing, China*

Guest Editor: Liping Zhou

POST-IR IRSL CHRONOLOGY OF PALEO-LACUSTRINE SEDIMENTS FROM YARDANGS IN THE Q AidAM BASIN, NE TIBETAN PLATEAU

ZHAOJING DING^{1,2}, LUPENG YU¹, ZHONGPING LAI^{2,3}, PING AN¹, XIAODONG MIAO¹,
RURU XU¹ and ZENGQI LIU¹

¹Luminescence Research Laboratory, Shandong Provincial Key Laboratory of Water and Soil Conservation & Environmental Protection, School of Resource and Environmental Sciences, Linyi University, Linyi 276000, China

²School of Earth Sciences, China University of Geosciences, Wuhan 430074, China

³Institute of Marine Science, Shantou University, Shantou 515063, China

Received 15 February 2019

Accepted 15 April 2020

Abstract: The Qaidam Basin preserves the largest Yardang field on Earth, and yardangs are intriguing landforms for studies of the paleo-environment and aeolian processes. Formation of yardangs involved both the initial lacustrine deposition and the subsequent wind-erosion processes. However, the timings of both processes in the Qaidam Basin are still controversial due to limited age data and unsuitable dating methodology. In this paper, we first compared two optical dating methods to determine the suitable one for the study area, then investigated the geomorphic processes based on the new ages. Two-step post-IR IRSL (pIRIR) and multi-elevated-temperature pIRIR (MET-pIRIR) methods of feldspar, were applied to date lacustrine sediments on the top parts of yardangs to decipher the transition time from depositional to an erosional environment. Comparisons of the two methods demonstrated that the influence from anomalous fading was very minimal thus negligible for MET-pIRIR method, as proved by the De plateau between MET-pIRIR₂₅₀ and MET-pIRIR₂₉₀; while the pIR50IR₂₅₀ signals suffered from fading obviously, which was difficult to be corrected due to the high De close to saturation. Consequently, the chronology in this study was based on the MET-pIRIR₂₅₀ method, potentially offering reliable ages of over 200 ka. Seven MET-pIRIR₂₅₀ ages of 201–336 ka suggested that a mega-Qaidam Lake (>2714 m a.s.l. on Google Earth) maintained until Marine Isotopic Stage (MIS) 7. The absence of sediments since ca. 200 ka implied wind-erosion and yardang formation since MIS6. This transition from lacustrine to a wind-erosion environment was interpreted as a response to the glacial-interglacial scale climatic changes.

Keywords: wind-erosion of Yardang, feldspar luminescence dating, anomalous fading, glacial-interglacial scale environmental change, Qaidam Basin, Qarhan Salt Lake.

1. INTRODUCTION

Yardang is a typical wind-erosional landform in the arid and hyper-arid areas on the Earth (Goudie, 2007; Al-Dousari *et al.*, 2009), and is a common landform on the Mars as well (Xiao *et al.*, 2017, Anglés and Li, 2017; Wang *et al.*, 2018). Studies on the evolution of Yardang have made significant progress attributed to the development of methods, e.g. remote sensing and geographic information system (Goudie, 2007), exposure dating (Wu *et al.*, 2019) and erosion rate testing (Rohrmann *et al.*, 2013) of ^{10}Be .

The yardang field in the Qaidam Basin (QB), with an area of $3.88 \times 10^4 \text{ km}^2$, is the largest one on the Earth (Halimov and Fezer, 1989), and its extreme environments (high, cold, windy, arid and low pressure) make it an ideal terrestrial analogue site for aeolian geomorphologic studies on the Mars (Xiao *et al.*, 2017, Anglés and Li, 2017; Wang *et al.*, 2018). These yardangs indicate a transition from lacustrine to wind-eroded condition (Kapp *et al.*, 2011; Rohrmann *et al.*, 2013). The materials eroded from the yardangs can be redeposited into the downwind dune fields and loess in the eastern and southern QB (Yu and Lai, 2012, 2014; Yu *et al.*, 2013, 2015a, 2015b) and also in the Chinese Loess Plateau (CLP) (Bowler *et al.*, 1987; Kapp *et al.*, 2011; Pullen *et al.*, 2011; Rohrmann *et al.*, 2013; Lai *et al.*, 2014; Mischke *et al.*, 2015). However, the time of the transition from lacustrine and wind-erosion environmental, *i.e.*, the formation of yardangs, is still controversial. Earlier studies based on ^{14}C dating proposed a mega-Qaidam Lake during Marine Isotopic Stage (MIS) 3 (Chen and Bower, 1986; Zhang *et al.*, 2008), while the paleo-lacustrine sediments were dated to MIS5 by quartz Optically Stimulated Luminescence (OSL) dating (Lai *et al.*, 2014). Depending on the regional geomorphological evolution, the formation time of the yardangs (onset of wind-erosion) is closely related to the above issues, but still unclear.

OSL dating has been applied in the QB to date both fluvial/lacustrine and aeolian sediments (e.g., Sun *et al.*, 2010; Yu and Lai, 2012, 2014; Yu *et al.*, 2013, 2015b, 2016; Lai *et al.*, 2014). The quartz OSL signals, however, have been shown to saturate at relatively low doses of $\sim 150 \text{ Gy}$ on the CLP (Buylaert *et al.*, 2008; Chapot *et al.*, 2012), making it difficult to date the old (Pleistocene) lacustrine sediments in yardangs. Alternatively, the post-IR IRSL (pIRIR) dating of feldspars (Thomsen *et al.*, 2008), with a much higher saturate dose up to $\sim 1000 \text{ Gy}$ (Li *et al.*, 2018), has the potential advantages. Two-step pIRIR procedure (Thomsen *et al.*, 2008; Buylaert *et al.*, 2009) and multiple-elevated-temperature (MET) pIRIR procedure (Li and Li, 2011) have been proposed for feldspar pIRIR dating. Compared with the two-step pIRIR signals, the MET-pIRIR signals are less affected by fading but more difficult to be sufficiently bleached (Li and Li, 2012). However, no studies have shown which method is more suitable for such old sediments on the Tibetan

Plateau (TP). In this study, both methods were applied to determine a proper dating method for the lacustrine sediments from yardangs in the central QB, and to offer reliable chronology for the transition from lacustrine to wind-erosional environment and geomorphic evolution (yardang formation).

2. YARDANGS AND SAMPLES

QB is a tectonically controlled depression on the northeastern TP and surrounded by Mountains (Fig. 1). Nowadays, with a potential-evaporation/precipitation ratio of > 100 (Chen and Bowler, 1985, 1986; Bowler *et al.*, 1986), the extreme arid QB is dominated by playas/salt lakes and aeolian landforms. Modern meteorological data of 1971–2010 showed that the gale (wind speed $\geq 17 \text{ m/s}$) days reached 163 d/yr (Zhang *et al.*, 2014). Consequently, the wind erosion prevails and now yardangs cover *ca.* 1/3 area of the QB (Kapp *et al.*, 2011), with the estimated erosion rate as $\sim 0.125\text{--}0.29 \text{ mm/yr}$ (Kapp *et al.*, 2011; Rohrmann *et al.*, 2013) during the Quaternary. Yardang orientations change from NNW-SSE in the northwestern part to WNW-ESE in the southeastern part corresponding to the changes of wind direction (Li *et al.*, 2016; Hu *et al.*, 2017).

Some road-cut sections display the stratigraphy of yardangs (Fig. 2), with heights of $\sim 5\text{--}15 \text{ m}$, in the north of Qarhan Salt Lake (QSL) region. All these sections show horizontal or sub-horizontal strata with greenish, reddish and brownish layers, indicating typical lacustrine characteristics. The horizontal beddings demonstrate the limited influences from tectonic activities, *i.e.*, not too old, which was an important criterion for us to identify the relatively young stratigraphy in the field. To reveal the termination of lacustrine environment, OSL samples were mainly taken from the upper part of the higher yardangs, which might be less eroded. Seven OSL samples were collected from five sites (Fig. 1) with the top elevations of 2643–2671 m measured by differential GPS, which is $\sim 50 \text{ m}$ lower than that derived from Google Earth (2704–2721 m). Samples YD3-A, YD6-B and YD7-C are mainly composed of clay and silt, and YD6-A, YD7-B, YD8-B and YD9-B are mainly composed of silt and fine sand. The details of section lithofacies and sampling locations are shown in Table 1.

3. MATERIALS AND MEASUREMENTS

Samples were treated with HCl and H_2O_2 to remove carbonates and organic materials, respectively. The fraction of 4–11 μm (by settling samples using Stokes' Law) or 150–180 μm (by wet sieving) were selected according to the grain composition of sediments. K-feldspars (KF) were extracted from the coarse grains (150–180 μm) by density separation ($2.53\text{--}2.58 \text{ g/cm}^3$) using sodium polytungstate and without HF etching. The KF were made

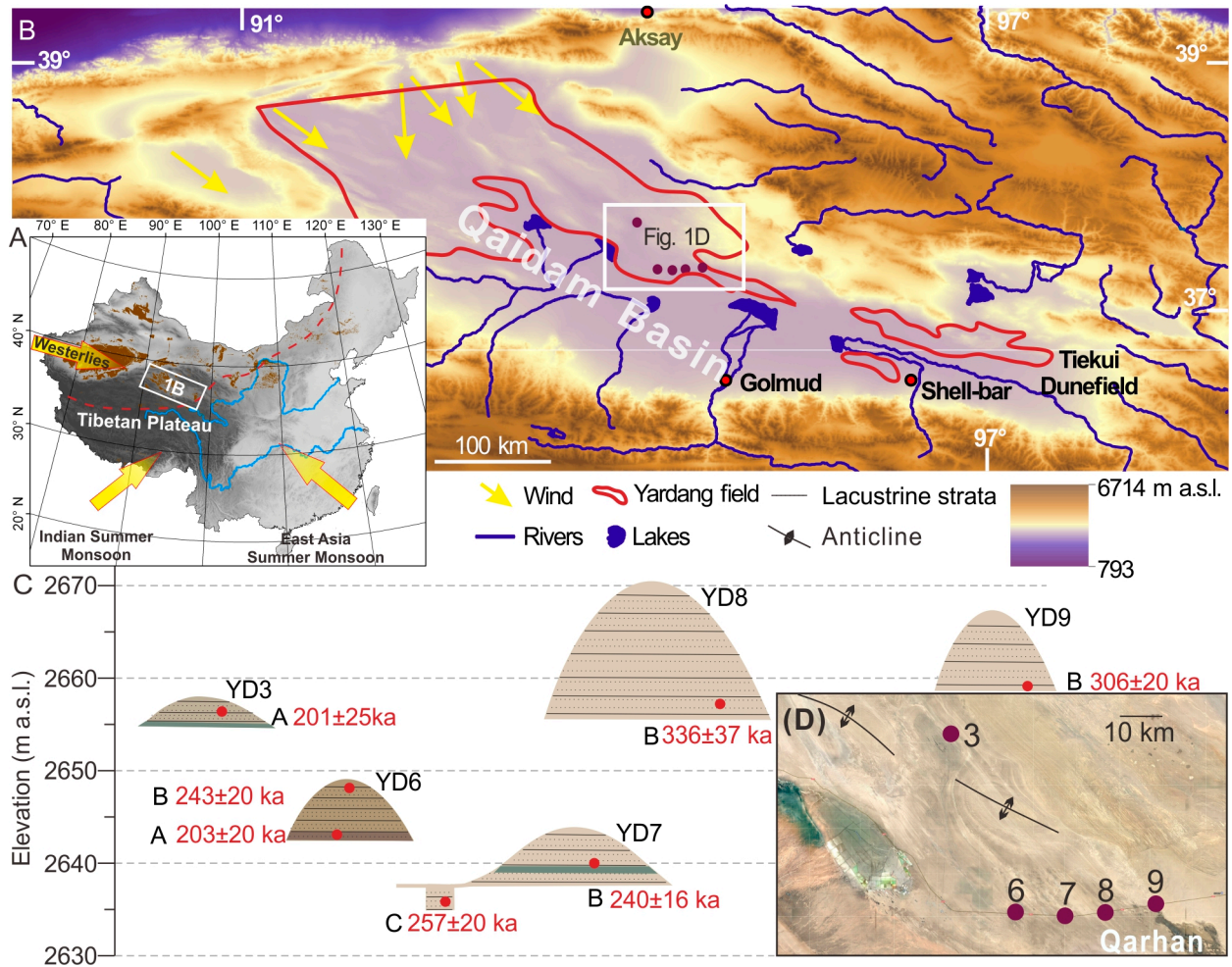


Fig. 1. Landform (A-B) and sampled yardangs (C-D) in the Qaidam Basin. The elevations measured by differential GPS were used in Fig. 1C as it's more accurate.

Table 1. Age results of MET-pIRIR₂₅₀ with sample informations.

Sample	Lithofacies and structures	Yardang height (m)	Grain size (μm)	Depth (m)	Altitude (m)	Water content (%)	Environmental Dose Rate (Gy·ka ⁻¹)	MET-pIRIR ₂₅₀	
								De (Gy)	Age (ka)
YD3-A	Gray-brown clay, horizontal stratification	3	4–11	1+10 ^a	2656	15±5	5.4±0.6	1082±75	201±25
YD6-A	Gray-brown sandy clay, horizontal stratification	5.5	63–90	5+10 ^a	2644	15±5	4.8±0.3	980±55	203±20
YD6-B	Gray-brown clay, horizontal stratification		4–11	0.5+10 ^a	2648	15±5	4.1±0.2	985±74	243±20
YD7-B	Reddish-brown sandy clay, plane-parallel lamination	6	150–180	4+10 ^a	2640	15±5	2.8±0.1	673±37	240±16
YD7-C	Clay-bank clay, horizontal stratification		4–11	8+10 ^a	2636	15±5	4.2±0.2	1061±75	257±20
YD8-B	Yellow sand, plane-parallel lamination	15	150–180	13+10 ^a	2658	15±5	2.7±0.1	902.2±92.2	336±37
YD9-B	Yellow sand, plane-parallel lamination	8	150–180	8+10 ^a	2659	15±5	2.6±0.1	790.0±39.5	306±20

^aAn additional depth of 10 m was given to the samples in the calculation.

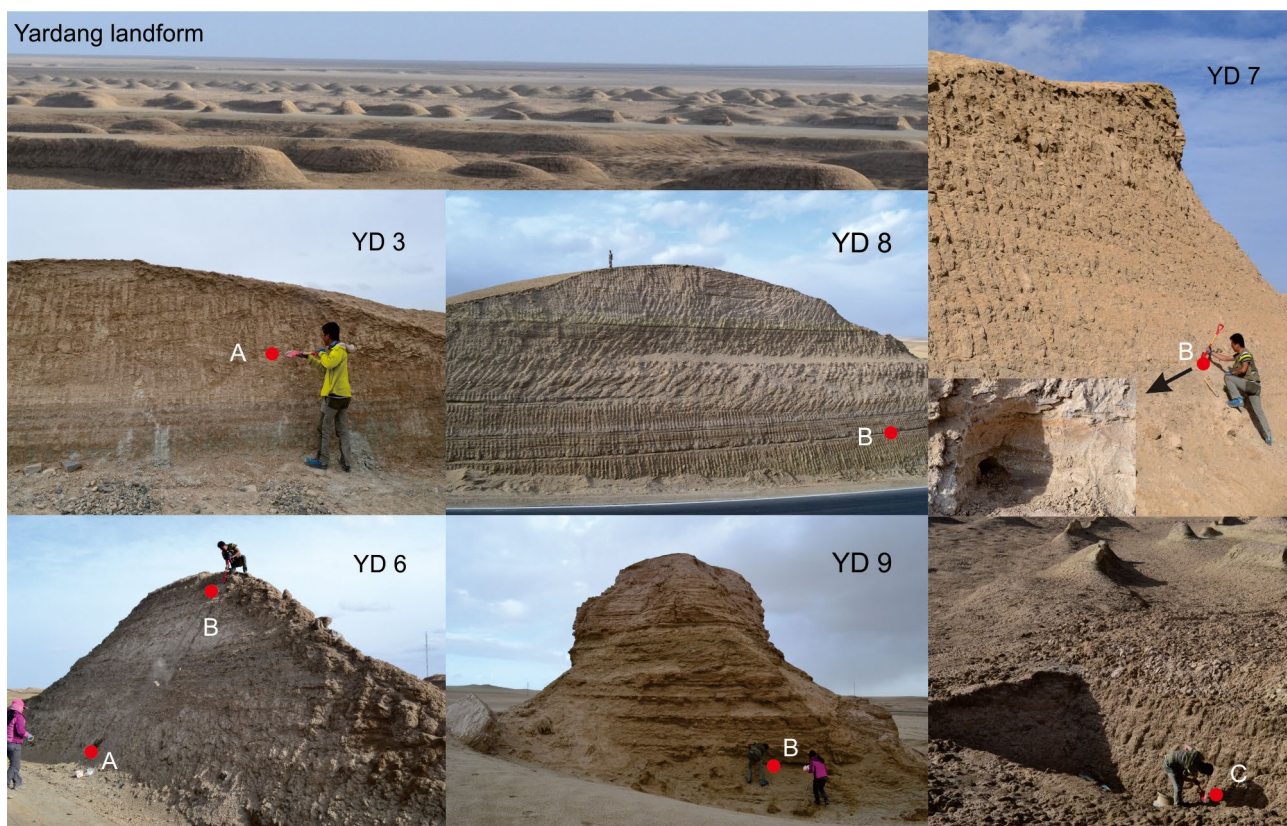


Fig. 2. Yardang landform and sampling sections. The filled red circles denote the positions of sampling.

into small aliquots with a diameter of 2 mm, and the 4–11 μm fractions were made into large aliquots.

Luminescence measurements were made by automated Risø TL/OSL readers (DA-20) with $^{90}\text{Sr}/^{90}\text{Y}$ beta sources in Linyi University and China University of Geoscience (Wuhan). The IRSL signals were detected through Schott BG39 and BG3 filters combination. A heating rate of $5^\circ\text{C}/\text{s}$ in a nitrogen atmosphere was employed, followed by a pause of 10 s. The L_x and T_x were calculated using the initial 8 s signals of decay curves, with a subtraction of the last 100 s from 500 s for two-step pIRIR or the last 20 s from 100 s for MET-pIRIR. The dose rates and ages were calculated with the online Dose Rate Calculator (Durcan *et al.*, 2015). The internal K contents of KF were estimated as $12.5 \pm 0.5\%$ (Huntley and Baril, 1997). The a -value is 0.15 ± 0.05 for coarse grain size (Balescu and Lamothe, 1994), and 0.086 ± 0.038 for fine grain size (Rees-Jones, 1995). The measured water contents range only 0.31–5.47%, which are extremely low, especially for the paleo-lacustrine sediments. Combining their saturated water content of ~20–40% and the alternation of humid and arid environments during the past interglacial-glacial cycles, an average range of measured and saturate values, $15 \pm 5\%$, were estimated for these lacustrine sediments during their burial history. Taking the average wind erosion rate of 0.125 mm/yr (Rohrman *et al.*, 2013) into account, an

additional depth of 10 m was added to the sample depths to calculate the ages. This estimation should be reasonable because the results increase slightly when the depth increases > 10 m. Five samples (YD6-B, YD7-C, YD7-B, YD8-B and YD9-B) are used for methodological studies illustrated as follow.

4. METHODS AND EXPERIMENTS

MET- pIRIR

In this study, the IR stimulations at 50, 100, 150, 200, 250, and 290°C with a preheat of 320°C were applied (Table 2a) after Li and Li (2011), using a single-aliquot regenerative-dose (SAR) protocol (Murray and Wintle, 2000; 2003), which is also for the two-step pIRIR.

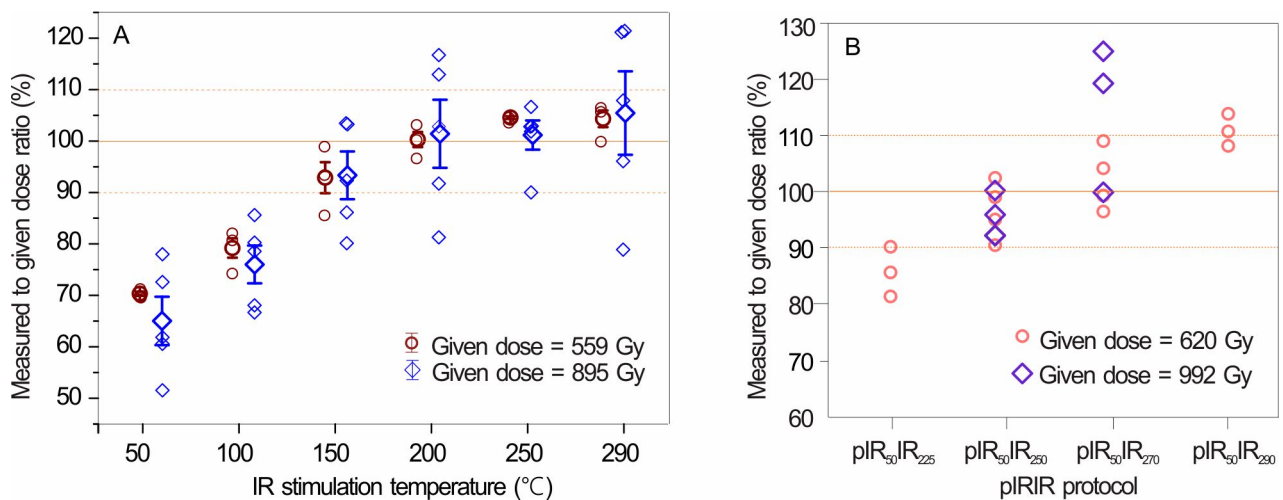
Dose recovery test and luminescence properties

To examine the reliability of D_e estimation, dose recovery test was conducted on a well-bleached modern sand sample in the QSL region. For KF (150–180 μm), laboratory doses of 559 and 895 Gy were given to 3 and 5 aliquots (diameter of ~3 mm), respectively, followed by a measurement protocol in Table 2a. The ratios of measured to given dose for different MET-pIRIR signals were shown in Fig. 3A, which displays a plateau from 200°C to 290°C , with the best recovery ratio at 250°C .

Table 2. Age results of MET-pIRIR₂₅₀ with sample informations.

(a) MET-pIRIR ₂₅₀ of Feldspar		(b) pIR ₅₀ IR ₂₅₀ of Feldspar	
Step	Treatment	Measured	Treatment
1	Dose	-	Dose
2	Preheat 320°C for 60 s	-	Preheat 280°C for 60 s
3	IRSL 50°C for 100 s	-	IRSL 50°C for 500 s
4	IRSL 100°C for 100 s	-	IRSL 250°C for 500 s
5	IRSL 150°C for 100 s	-	Test dose
6	IRSL 200°C for 100 s	-	Preheat 280°C for 60 s
7	IRSL 250°C for 100 s	L _x	IRSL 50°C for 500 s
8	IRSL 290°C for 100 s	-	IRSL 250°C for 500 s
9	Test dose	-	Return to step 1
10	Preheat 320°C for 60 s	-	
11	IRSL 50°C for 100 s	-	
12	IRSL 100°C for 100 s	-	
13	IRSL 150°C for 100 s	-	
14	IRSL 200°C for 100 s	-	
15	IRSL 250°C for 100 s	T _x	
16	IRSL 290°C for 100 s	-	
17	IRSL 320°C for 100 s	-	
18	Return to step 1		

Luminescence properties of MET-pIRIR signals were investigated (Fig. 4). Fig. 4A displayed a similar decay rate between fine-grain polymineral and coarse-grain KF for the MET-pIRIR₂₅₀ signals. Fig. 4B showed an obvious D_e plateau between the stimulation temperature of 250 and 290°C, and a continuous increase from 50°C to 200°C. Fig. 4C–4F suggested a saturate dose of beyond 1200 Gy for the MET-pIRIR₂₅₀ signals, while that of the MET-pIRIR₂₉₀ signals is lower (Fig. 4C). Fig. 4D also illustrated that the DRCs of MET-pIRIR₂₅₀ derived from different aliquots are similar to their SGC derived from 3–4 DRCs for each sample, suggesting that the SGC method (Roberts and Duller, 2004; Lai and Ou, 2013) could be applied for these samples.

**Fig. 3.** Dose recovery test for MET-pIRIR protocols (A) and two-step pIRIR protocols (B).

Bleaching behaviour and residuals

To test the bleaching behaviour of MET-pIRIR signals of the paleo-lacustrine sediments, six groups of small aliquots were exposed to natural sunlight for different bleaching durations in Linyi (118°17' E, 35°07' N) in August 2018. The results (Fig. 5) indicated that the residual doses of MET-pIRIR signals at different stimulation temperatures all decreased with the increase of bleaching time. Moreover, residual signals of 250°C were bleached to 4.2% of the natural signals after 3 hrs bleaching, and the residual dose dropped to only 21.8 Gy (equal to *ca.* 6.2 ka with an average dose rate of 3.5 Gy/ka) after 24 hrs. This suggested the MET-pIRIR₂₅₀ signals could be well bleached in the QB, where the insolation is of over 5000 MJ/ (m²·a), 50–100% higher than in the low-altitude areas of the same latitude (Zheng and Zhao, 2017).

Two-step pIRIR

To decrease the influence of the undetectable carry-over charge (Kars *et al.*, 2014) and probable anomalous fading, an extended stimulation time of 500 s and a big test dose of 248 Gy were applied (Colarossi *et al.*, 2018). The latter has the effect of increasing D₀ values as well (Qin and Zhou, 2012; Colarossi *et al.*, 2018). The protocol for pIR₅₀IR₂₅₀ determined by dose recovery test was shown in Table 2b.

Dose recovery test and luminescence properties

Twenty aliquots of sample YD9-B were bleached by sunlight for 24 hrs for dose recovery test. Preheat temperatures of 250–320°C (250, 280, 300, and 320°C) were applied, followed by a first IR stimulation at 50°C, and a second IR stimulation at 225, 250, 270, and 290°C, respectively. The first dose of 620 Gy was given, and 3–4 aliquots for each temperature were measured. Without the

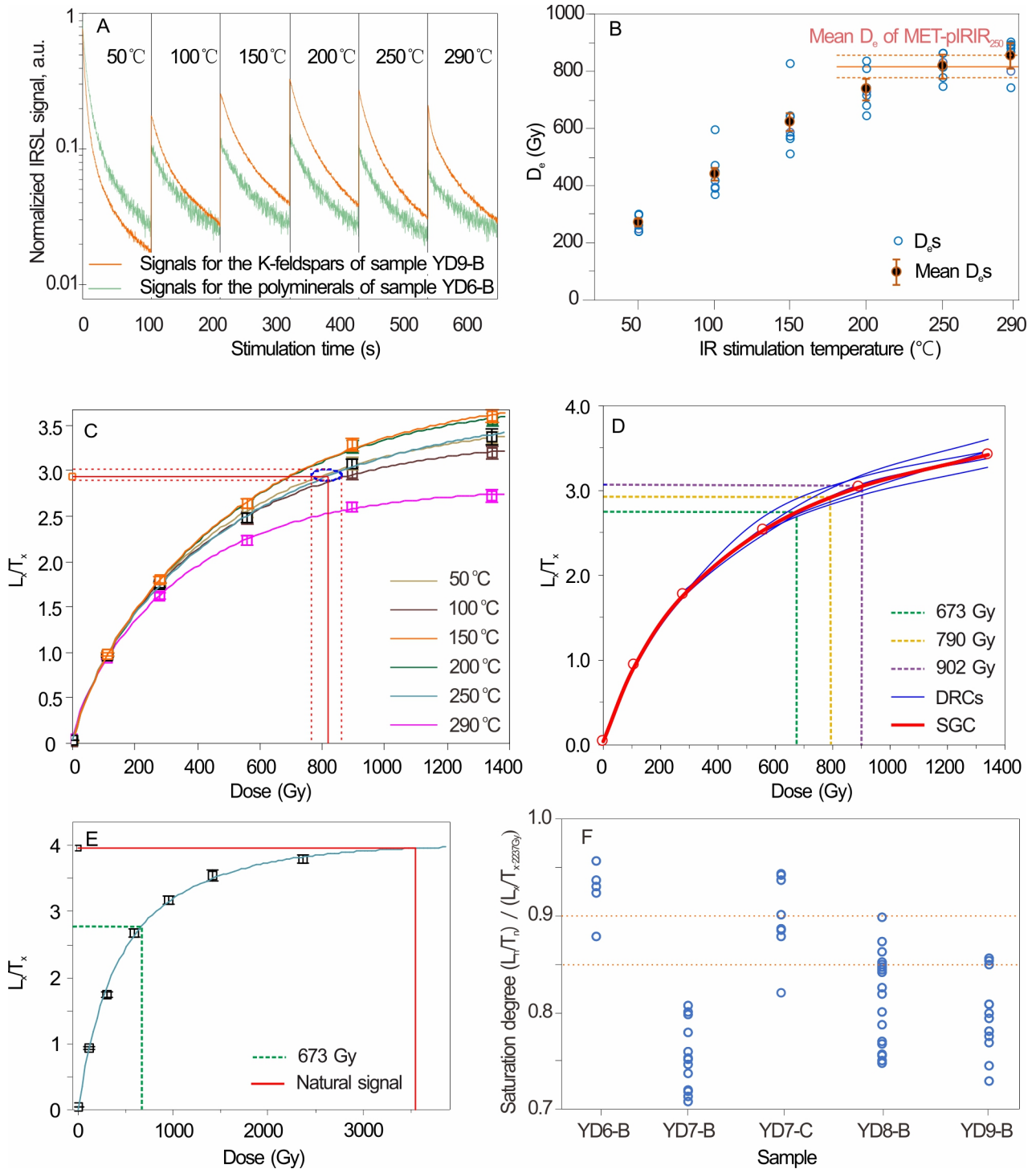


Fig. 4. Luminescence properties of MET-pIRIR signals using the protocol in Table 2a: (A) Decay curves of K-feldspars and polyminerals, (B) D_e s at different stimulation temperatures and (C) corresponding DRCs for sample YD9-B, (D) DRCs of MET-pIRIR₂₅₀ signals of sample YD8-B and their SGC. (E) DRC of MET-pIRIR₂₅₀ signal of sample of field saturation in the QB, using two exponential function. (F) Saturate ratio. It is expressed by the ratios of (L_x/T_n) (natural signals) and (L_x/T_n) , the latter is derived from ~1969 Gy and field saturated dose for fine-grain polyminerals and coarse-grain K-feldspars, respectively (no fine-grain sample of field saturation were collected).

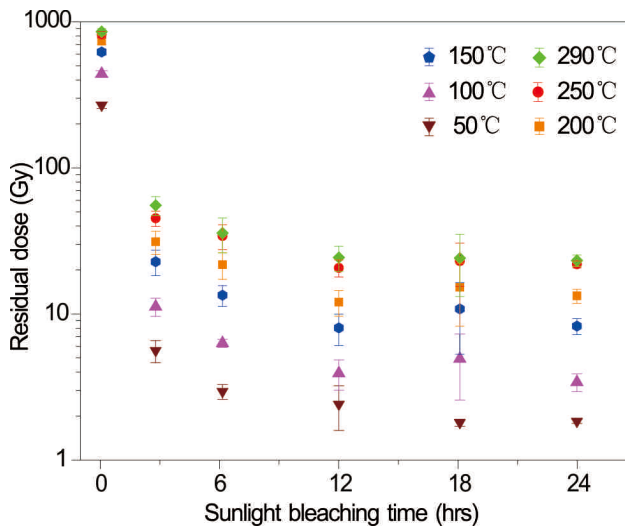


Fig. 5. Residual doses as a function of sunlight bleaching time for the MET-pIRIR signals of sample YD9-B.

subtraction of residual doses (for details see Section 4 – Two-step pIRIR – Residuals and anomalous fading test) from $D_{e,s}$, the measured/given dose ratios (**Fig. 3B**) suggest the results of pIR₅₀IR₂₅₀ and pIR₅₀IR₂₇₀ are acceptable. Another dose recovery test of 992 Gy (**Fig. 3B**) and the smaller residual dose further confirmed that the pIR₅₀IR₂₅₀ signals behaved better.

The signals of the nature dose and test dose of the pIR₅₀IR₂₅₀ signals can decay to a low level after stimulation of 500 s (**Fig. 6A**), which was further confirmed by the relative stable sensitivity changes during the SAR cycles (**Fig. 6C**). **Fig. 6B** displayed that the natural dose of IRSL₅₀ is much smaller than the pIR₅₀IR₂₅₀, which was attributed to the fading of the IRSL₅₀. The SGC of the pIR₅₀IR₂₅₀ signals coincide with their DRCs as well.

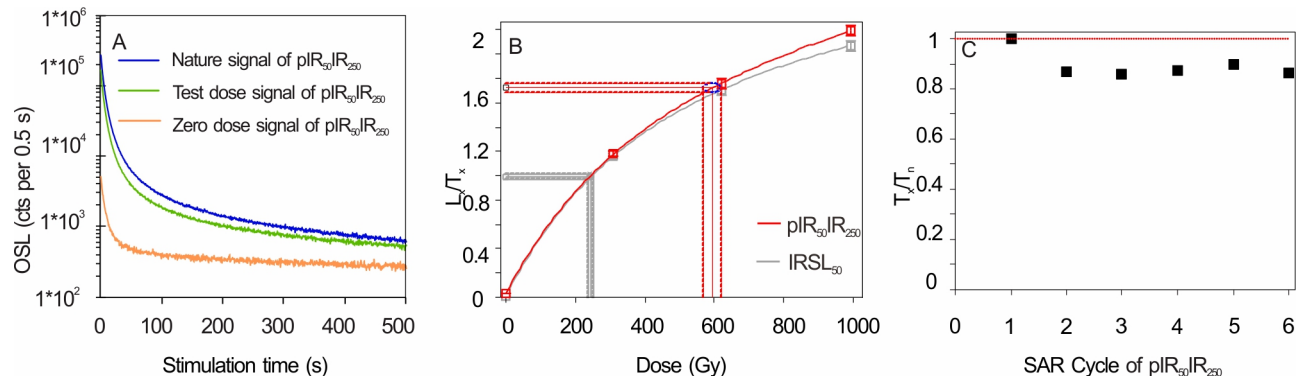


Fig. 6. Luminescence properties of two-step pIRIR signals. (A) Decay curves of IR₅₀IR₂₅₀ signals, (B) DRCs and natural doses of IRSL₅₀ and IR₅₀IR₂₅₀, and (C) Sensitivity changes of pIR₅₀IR₂₅₀ for sample YD9-B.

Residuals and anomalous fading test

The residual dose determination was conducted on six sunlight-bleached (24 hrs) aliquots for each temperature, and the results of pIR₅₀IR₂₂₅, pIR₅₀IR₂₅₀, pIR₅₀IR₂₇₀ and pIR₅₀IR₂₉₀ were 6.2, 8.2, 11.6, and 14.2 Gy, respectively. The anomalous fading rate measurements were conducted on three measured aliquots (YD9-B), and the single aliquot measurement procedures were similar to Auclair *et al.* (2003), but based on the pIR₅₀IR₂₅₀ protocol (**Table 2b**). The same regenerative dose of 124 Gy followed by a preheat of 280°C was given before different storage times. Using the software of Analyst, a series of L_x/T_x values as a function of storage times were plotted for the g-value that is normalised to a t_c of 2 days (Huntley and Lamothé 2001). As shown in **Fig. 7A** and **7B**, the measurements of 3 aliquots show a mean g-values of 1.54 ± 0.20 %/decade for the pIR₅₀IR₂₅₀, and 2.97 ± 0.66 %/decade for the IRSL₅₀.

5. RESULTS AND DISCUSSION

Comparisons of MET-pIRIR₂₅₀ and pIR₅₀IR₂₅₀ dating

MET-pIRIR₂₅₀

For MET-pIRIR, a plateau of similar D_e values obtained at higher temperatures could suggest negligible anomalous fading (Li and Li, 2011). In this study, the D_e plateaus between 250 and 290°C (**Fig. 4C**) suggested negligible fading as well. The MET-pIRIR₂₅₀ signal was chosen because its residual dose was smaller and the signal level was higher than that of the MET-pIRIR₂₉₀.

The measured residual dose of MET-pIRIR₂₅₀, 21.8 Gy, (**Fig. 5**) was subtracted from the mean $D_{e,s}$ of each sample for correction. In this study, any aliquots without D_e plateau between MET-pIRIR₂₅₀ and MET-pIRIR₂₉₀, which suggested insufficient bleaching

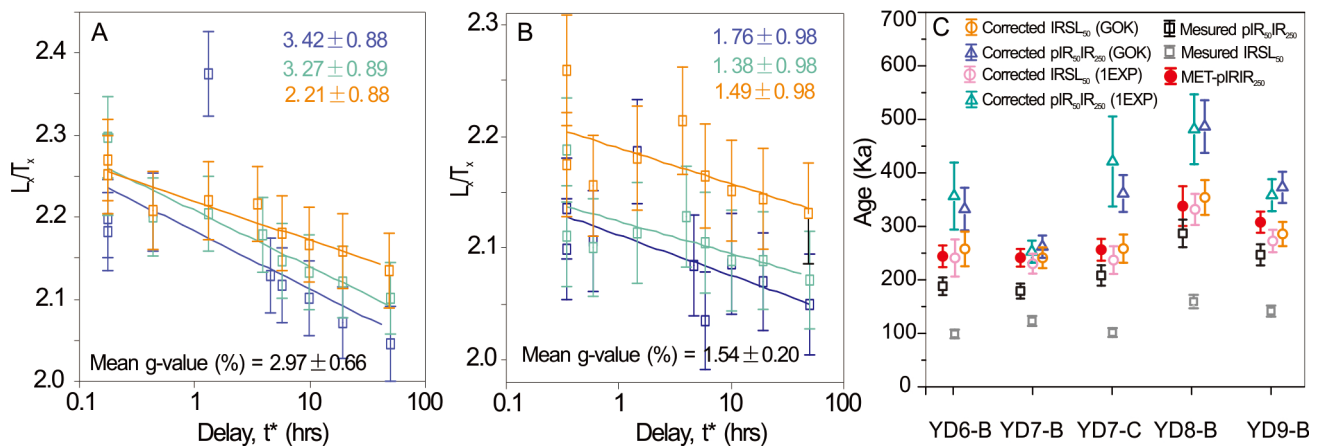


Fig. 7. Fading test of IRSL₅₀ (A) and $pIR_{50}IR_{250}$ (B) signals of sample YD9-B, and Comparison of multiple age results (C).

(Fu, 2014), were rejected. Furthermore, the DRCs fitted with double exponentials (Fig. 4D) can offer higher saturate dose of beyond 1200 Gy for MET- $pIR_{50}IR_{250}$ signals. This was supported by the conclusion of Galbraith and Roberts (2012) that much higher D_e values could be estimated when the DRC was fitted accurately. A field saturated yardang sample offered a D_e of beyond 2237 Gy (Fig. 4E), suggesting the fading of the MET- $pIR_{50}IR_{250}$ signals was very minimal. If the normalised natural signals of the saturate sample ($L_s/T_n=3.961$) was regarded as the saturation level, the normalised natural signals (L_n/T_n) could be compared with it to evaluate the saturate ratio ($(L_n/T_n)/(L_s/T_n)$) for each coarse-grained aliquot (Fig. 4F). Due to the lack of field saturate sample for fine grains, the minimal laboratory saturation level (~1969 Gy, we did not make the DRC saturation) was used to estimate a maximal saturate ratio for each fine-grained aliquot. Most of the coarse-grain samples have the saturate ratios of below 85%. However, without independent age control, we are cautious with the results of ca. 900–1000 Gy. The success of dose recovery test of 895 Gy (Fig. 3A) further suggested that at least the results below 900 Gy were reliable. The comparison of the ages, stratigraphy and elevations among different sections also demonstrated the reliability of most of these ages, as interpreted in part 5.2. All the MET- $pIR_{50}IR_{250}$ ages are in Table 1.

$pIR_{50}IR_{250}$

The fading test (Fig. 7A-7B) offered a mean g-value of 1.54 ± 0.20 %/decade for $pIR_{50}IR_{250}$ signals. Some studies proposed that the fading correction for the $pIR_{50}IR_{225-290}$ is unnecessary because either their natural signals can reach saturate level (Thiel *et al.*, 2011; Liu *et al.*, 2016), or the uncorrected age could agree with the independent ages (Thiel *et al.*, 2011; Roberts, 2012). Thiel *et al.* (2011) proposed that the measured g-values (0.07 ± 0.78 to 2.00 ± 0.64 %/decade) for $pIR_{50}IR_{290}$ were artificial in the laboratory and should be ignored. In contrast, Li and Li

(2012) found that the anomalous fading would lead to underestimations for older samples (e.g., >500 Gy) with the $pIR_{50}IR_{290}$ method, while it is not a problem for younger samples. For our samples, the measured ages of $pIR_{50}IR_{250}$ were severely underestimated by even more than 20% compared to MET- $pIR_{50}IR_{250}$ ages. Based on the anomalous fading tests, ages of IRSL₅₀ and $pIR_{50}IR_{250}$ were calibrated according to the model of Huntley (2006) for our relative old samples. The calculations were conducted with the R. luminescence package (Kreutzer *et al.*, 2019), using the approaches in Kars *et al.* (2008) (a single-saturating exponential fit, 1EXP) and Guralnik *et al.* (2015) (a general-order kinetic fit, GOK), which had been evaluated for the fading-correction by King *et al.* (2018). The corrected results were shown in Fig. 7C, and Table 3 gives some details, including the samples' saturation level (*i.e.*, (n/N) is the samples' level of saturation for the natural state; $(n/N)_{SS}$ is the samples' level of saturation for field steady-state (King *et al.* 2018)), measured D_e , corrected D_0 , corrected D_e , corrected age. The comparisons of saturation level displayed that when the measured D_e s of $pIR_{50}IR_{250}$ reach ~700–800 Gy, results of 1EXP fitting showed saturation (e.g., sample YD6-B, YD7-C and YD8-B), but not GOK fitting (Table 3). This suggested that the fitting mode might affect the saturation of simulated DRCs, especially for old samples. Nevertheless, YD7-B and YD9-B can be determined to be unsaturated (Table 3), which confirms that such high underestimation of $pIR_{50}IR_{250}$ was caused by anomalous fading rather than natural saturation. This agrees with the result of Thomsen *et al.* (2011) that the extended duration of the prior IRSL₅₀ for beyond 100 s could not offer a significantly more stable $pIR_{50}IR_{290}$ signal. As shown in Fig. 7C, the ages of corrected IRSL₅₀ agreed with MET- $pIR_{50}IR_{250}$, however, except for YD7-B, the fading corrections of $pIR_{50}IR_{250}$ showed an overestimation (Fig. 7C), similar to the description of King *et al.* (2018). It might be related to a state near or already saturated (e.g. sample YD6-B, YD7-C and YD8-B), fitting modes and/or the

Table 3. The results corrected by *Huntley (2006)* method.

Function	Sample	IRSL ₅₀					
		(n/N)	(n/N) _{SS}	Measured D _e ^a (Gy)	Corrected D ₀ ^b (Gy)	Corrected D _e ^c (Gy)	Corrected Age ^d (ka)
1EXP	YD6-B	0.54±0.02	0.60±0.13	397±16	372±1	973±124	240±34
	YD7-B	0.43±0.01	0.58±0.14	345±11	465±1	642±29	229.0±19
	YD7-C	0.52±0.02	0.59±0.13	429±18	422±1	981±85	236±25.8
	YD8-B	0.48±0.01	0.57±0.14	427±14	479±1	886±49	330±29
	YD9-B	0.44±0.01	0.59±0.14	364±10	467±1	700±27	271±21
GOK	YD6-B	0.46±0.02	0.60±0.17	401±20	362±1	1040±110	256±32
	YD7-B	0.37±0.01	0.60±0.16	345±12	501±2	673±30	240±19
	YD7-C	0.34±0.01	0.62±0.15	423±21	463±3	1070±82	257±26
	YD8-B	0.40±0.01	0.57±0.12	428±17	494±1	945±59	352±32
	YD9-B	0.32±0.01	0.59±0.12	365±11	583±1	733±31	284±23
Function	Sample	IR ₅₀ IR ₂₅₀					
		(n/N)	(n/N) _{SS}	Measured D _e ^a (Gy)	Corrected D ₀ ^b (Gy)	Corrected D _e ^c (Gy)	Corrected Age ^d (ka)
1EXP	YD6-B	0.72±0.02	0.72±0.21	716±40	439±1	1440±2334	355±62
	YD7-B	0.57±0.02	0.71±0.2	491±18	483±1	705±33	252±21
	YD7-C	0.73±0.02	0.72±0.2	815±48	487±1	1744±328	419±84
	YD8-B	0.69±0.02	0.71±0.2	726±36	497±2	1286±151	480±65
	YD9-B	0.61±0.02	0.71±0.19	616±23	535±2	920±46	357±30
GOK	YD6-B	0.54±0.02	0.72±0.19	760±42	485±2	1342±133	331±40
	YD7-B	0.41±0.01	0.72±0.22	500±20	605±3	731±32	261±21
	YD7-C	0.31±0.01	0.72±0.23	862±54	800±11	1497±102	360±34
	YD8-B	0.52±0.02	0.71±0.19	766±45	549±2	1300±98	484±49
	YD9-B	0.24±0.01	0.72±0.24	633±28	1170±26	957±39	371±29

a. D_e calculated through measured DRC (King *et al.*, 2018).

b. D₀ for simulated natural DRC (King *et al.*, 2018).

c. D_e calculated through simulated natural DRC (King *et al.*, 2018).

d. Age calculated through simulated natural DRC (King *et al.*, 2018).

differences between laboratory dose response and natural dose response caused by different origins or chemical compositions (King *et al.*, 2018). As a result, the pIR₅₀IR₂₅₀ dating is affected by anomalous fading for our samples even for a prior IRSL₅₀ of 500 s, and the correction for anomalous fading needs further studies. Consequently, the chronology for the following discussion was based on the MET-pIRIR₂₅₀ ages.

pIRIR chronology for paleo-lacustrine sediments

Previous chronology of lacustrine sediments in the QB was mainly based on ¹⁴C dating during the past decades (e.g., Chen *et al.*, 1981; Chen and Bowler, 1986; Bowler *et al.*, 1986; Zhang *et al.*, 2008). A mega-Qaidam paleolake was proposed to exist during *ca.* 40–30 ka (MIS3) based on the ¹⁴C dating of shells in the shell-bar (Fig. 1B, 2703 m a.s.l. on Google Earth) in the southeastern QSL region (Chen and Bowler, 1986; Zhang *et al.*, 2008). However, the range of ¹⁴C dating is too young for the yardangs in the QB, and even the ¹⁴C ages of 25–40 ka were proved to be underestimated in the QB (Yu *et al.*, 2009; Lai *et al.*, 2014; Mischke *et al.*, 2015; Yu *et al.*, 2018). Lai *et al.* (2014) dated the shell-bar to MIS5 (~100–110 ka) based on quartz OSL. While the upper

dating limit of quarts OSL (*ca.* 150 Gy on the CLP (Buylaert *et al.*, 2008; Chapot *et al.*, 2012)) implied that this result might also be underestimated. The feldspar MET-pIRIR₂₅₀, in this study, offered seven paleo-lacustrine ages ranged from *ca.* 200 to 340 ka in the northern QSL region (Table 1), demonstrating a mega-Qaidam paleolake existed in QSL during and prior to MIS 7.

The new MET-pIRIR₂₅₀ ages from this paper, together with the elevations of sections and samples, were displayed in Fig. 1C. The purpose of this study is to explore the termination time of the lacustrine environment. Consequently, we tried to investigate the ages of the highest yardangs in different regions. Based on the distribution, stratigraphy and ages, the five sections could be classified as three regions, the northern region (YD3), middle region (YD6 and YD7) and the eastern region. The YD6 and YD7 sections are close in distance and elevation. The D_e of YD7-B was only 673 Gy, which was far from saturation (Fig. 4D–4F), and consequently, its age of 240±16 ka is considered reliable. The YD6 section, at a higher elevation than YD7, should be younger than the latter. The YD6 presented similar ages with YD7 (reverse, but the same within errors), and we took their average age of 223±20 ka. As a result, the termination of the lacustrine environment in the middle region was after 220 ka. This

also agrees with the YD3 section in higher elevation and with younger ages (201 ± 25 ka). In this case, we can conclude that the lacustrine environment in the middle and northern regions terminated after *ca.* 200 ka, the MIS7. The low D_e of YD7-B further suggested these similar ages on similar elevation were less affected by fading and reliable. The YD8 and YD9 sections located at a higher elevation, and the D_e of YD9-B, 790 Gy, suggested the ages of MIS 9 should also be reliable. However, the samples cannot well present the latest time of lakes because they were not taken from the top of the yardangs, and consequently, it is unnecessary to make much interpretation on these two samples here.

Implications for yardang development

Taking into account that the previous radiocarbon ages (MIS3, Chen and Bowler, 1986; Zhang *et al.*, 2008) and quartz OSL ages (MIS5, Lai *et al.*, 2014) of the palaeo-lacustrine sediments are possible to be underestimated (Yu *et al.*, 2009; Lai *et al.*, 2014; Mischke *et al.*, 2015; Yu *et al.*, 2018; Buylaert *et al.*, 2008; Chapot *et al.*, 2012), there is no robust chronological evidence supporting the existence of mega-Qaidam paleolake since MIS6 at present. Additionally, the large-scale expansion of the Tiekui Dunefield (Fig. 1B), at the eastern end of the QB, suggested that there should be no mega lake in the QB during the most time from MIS6 to the early Holocene (Yu *et al.*, 2019). Even during MIS5, when the climate should be relatively humid, there were still dune activities during MIS5d and MIS5b (Yu *et al.*, 2019). Therefore, it is reasonable to infer that the mega-lake maintained till MIS7, and the severe wind-erosion and the widespread yardang formation in the QSL region started since MIS6. The eroded materials should have contributed to the expansions of the Tiekui Dunefield in the downwind direction of the QB since MIS6 (Yu *et al.*, 2019). The mega-Qaidam Lake demonstrated a humid climate during MIS7, while the severe wind erosion of yardangs and the expansion of the Tiekui Dunefield both indicated arid and windy climate during MIS6. The comparisons among lacustrine ages (Fig. 8A–8B), $\delta^{18}\text{O}$ records of stalagmites in Asain Summer Monsoon (ASM) influenced region (Fig. 8C, Cheng *et al.*, 2016), summer insolation of 30°N (Fig. 8D, Berger and Loutre, 1991), and sea level changes (Fig. 8E, Spratt and Lisiecki, 2016) suggested the mega-Qaidam Lake developed under the warm and humid climate during MIS7, while the transition to arid climate might result from the retreat of ASM and strengthening of the westerlies (An *et al.*, 2012) during MIS6. This suggested the palaeoenvironmental changes in glacial-interglacial scale in the QB, however, these limited data were not sufficient to support further discussions about the relevant mechanisms and processes, and more detailed studies are needed in future.

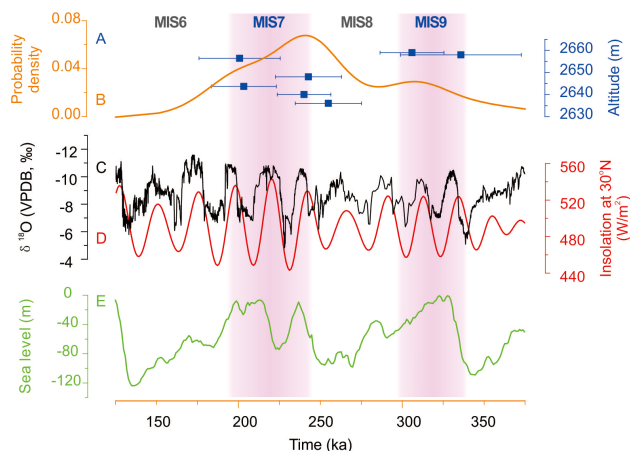


Fig. 8. (A) Scatter diagram of lacustrine ages against altitudes. (B) Probability density of lacustrine ages. (C) The composite $\delta^{18}\text{O}$ record of stalagmites (Cheng *et al.*, 2016). (D) Insolation at 30°N (Berger and Loutre, 1991). (E) Composite sea level stack (Spratt and Lisiecki, 2016).

6. CONCLUSIONS

Two main conclusions were drawn from this study: one is to find a suitable dating method, and the other is to infer the geomorphic processes based on the new ages. Methodology study suggests that the pIRIR dating is suitable for the paleo-lacustrine sediments in the QB, for both fine-grained polymineral samples and coarse-grain KF. The MET-pIRIR₂₅₀ signals could be well bleached and were less affected by fading as demonstrated by a D_e plateau. For pIR₅₀IR₂₅₀, fading correction is necessary, but the correction method for such old samples needs further studies. Thus, the results of MET-pIRIR₂₅₀ dating were used to explore the termination time of the lacustrine environment.

For the geomorphic processes of the yardang formation, the ages of ~ 200 – 340 ka from lacustrine sediment reveal that the mega-Qaidam paleolake existed during and prior to MIS7. The most recent extensive formation of yardangs in the northern QSL region might start since MIS6.

ACKNOWLEDGMENTS

This study was supported by National Scientific Foundation of China (NSFC41761144073, 41672167, and 41462006), Natural Science Foundation of Shandong Province (2015ZRB01ANY) and Shandong Provincial Key Laboratory of Water and Soil Conservation and Environmental Protection (STKF201930). We thank Dr. Jintang Qin for his discussion on the revised manuscript, and Tianyuan Chen, Yixuan Wang, and Qi Zhao for their help in the field.

REFERENCES

- Al-Dousari AM, Al-Elaj M, Al-Enezi E and Al-Shareeda A, 2009. Origin and characteristics of yardangs in the Um Al-Rimam depressions (N Kuwait). *Geomorphology* 104: 93–104, DOI 10.1016/j.geomorph.2008.05.010.
- An Z, Colman SM, Zhou W, Li X, Brown ET, Jull AJT, Cai Y, Huang Y, Lu X, Chang H, Song Y, Sun Y, Xu H, Liu W, Jin Z, Liu X, Cheng P, Liu Y, Ai L, Li X, Liu X, Yan L, Shi Z, Wang X, Wu F, Qiang X, Dong J, Lu F and Xu X, 2012. Interplay between the Westerlies and Asian monsoon recorded in Lake Qinghai sediments since 32 ka. *Scientific Reports* 2: 619, DOI 10.1038/srep00619.
- Anglés A and Li YL, 2017. The western Qaidam Basin as a potential Martian environmental analogue: an overview. *Journal of Geophysical Research: Planets* 122: 856–888, DOI 10.1002/2017JE005293.
- Auclair M, Lamothe M and Huot S, 2003. Measurement of anomalous fading for feldspar IRSL using SAR. *Radiation Measurements* 37(4–5): 487–492, DOI 10.1016/s1350-4487(03)00018-0.
- Balescu S and Lamothe M, 1994. Comparison of TL and IRSL age estimates of feldspar coarse grains from waterlain sediments. *Quaternary Science Reviews* 13(5–7): 437–444, DOI 10.1016/0277-3791(94)90056-6.
- Berger A and Loutre MF, 1991. Insolation values for the climate of the last 10 million years. *Quaternary Science Reviews* 10(4): 297–317, DOI 10.1016/0277-3791(91)90033-Q.
- Bowler JM, Chen KZ and Yuan BY, 1987. Systematic variations in loess source areas: Evidence from Qaidam and Qinghai basins, western China, in Tungsheng, L., ed., *Aspects of Loess Research*. China Ocean Press, Beijing: 39–51.
- Bowler JM, Huang Q, Chen KZ, Head MJ and Yuan BY, 1986. Radiocarbon dating of playa-lake hydrologic changes: Examples from northwestern China and central Australia. *Palaeogeography, Palaeoclimatology, Palaeoecology* 54: 241–260, DOI 10.1016/0031-0182(86)90127-6.
- Buylaert JP, Murray AS, Thomsen KJ and Jain M, 2009. Testing the potential of an elevated temperature IRSL signal from K-feldspar. *Radiation Measurements* 44: 560–565, DOI 10.1016/j.radmeas.2009.02.007.
- Buylaert JP, Murray AS, Vandenberghe D, Vriend M, Corte FD and Haute PVD, 2008. Optical dating of Chinese loess using sand-sized quartz: Establishing a time frame for Late Pleistocene climate changes in the western part of the Chinese Loess Plateau. *Quaternary Geochronology* 3(1–2): 99–113, DOI 10.1016/j.radmeas.2009.02.007.
- Chapot MS, Roberts HM, Duller GAT and Lai ZP, 2012. A comparison of natural- and laboratory-generated dose response curves for quartz optically stimulated luminescence signals from Chinese Loess. *Radiation Measurements* 47(11–12): 1045–1052, DOI 10.1016/j.radmeas.2012.09.001.
- Chen KZ and Bowler JM, 1985. Study on sedimentary characteristics and paleoclimate evolution of qarhan salt lake in Qaidam Basin. *Science China: series B* 5: 79–89 (in Chinese).
- Chen KZ and Bowler JM, 1986. Late pleistocene evolution of salt lakes in the Qaidam basin, Qinghai province, China. *Palaeogeography, Palaeoclimatology, Palaeoecology* 54: 87–104, DOI 10.1016/0031-0182(86)90119-7.
- Chen KZ, Yang S and Zheng X, 1981. The salt lakes on the Qinghai-Xizang plateau. *Acta Geographica Sinica* 36(1): 13–21 (in Chinese with English abstract).
- Cheng H, Edwards RL, Sinha A, Spötl C, Yi L, Chen ST, Kelly M, Kathayat G, Wang XF, Li XL, Kong XG, Wang YX, Ning YF and Zhang HW, 2016. The asian monsoon over the past 640,000 years and ice age terminations. *Nature* 534(7609): 640–646, DOI 10.1038/nature18591.
- Colarossi D, Duller GAT and Roberts HM, 2018. Exploring the behaviour of luminescence signals from feldspars: Implications for the single aliquot regenerative dose protocol. *Radiation Measurements* 109: 35–44, DOI 10.1016/j.radmeas.2017.07.005.
- Durcan JA, King GE and Duller GAT, 2015. DRAC: Dose Rate and Age Calculator for trapped charge dating. *Quaternary Geochronology* 28: 54–61, DOI 10.1016/j.quageo.2015.03.012.
- Fu X, 2014. The D e (T, t) plot: A straightforward self-diagnose tool for post-IR IRSL dating procedures. *Geochronometria* 41: 315–326, DOI 10.2478/s13386-013-0167-9.
- Galbraith RF and Roberts RG, 2012. Statistical aspects of equivalent dose and error calculation and display in OSL dating: An overview and some recommendations. *Quaternary Geochronology*, 11: 1–27, DOI 10.1016/j.quageo.2012.04.020.
- Guralnik B, Li B, Jain M, Chen R, Paris RB, Murray AS, Li SH, Pagonis P and Herman F, 2015. Radiation-induced growth and isothermal decay of infrared-stimulated luminescence from feldspar. *Radiation Measurements* 81: 224–231, DOI 10.1016/j.radmeas.2015.02.011.
- Goudie AS, 2007. Mega-Yardangs: A Global Analysis. *Geography Compass* 1(1): 65–81, DOI 10.1111/j.1749-8198.2006.00003.x.
- Halimov M and Fezer F, 1989. Eight yardang types in central Asia. *Zeitschrift Fur Geomorphologie* 33: 205–217.
- Hu CQ, Chen NH, Kapp P, Chen J, Xiao A and Zhao Y, 2017. Yardang geometries in the Qaidam Basin and their controlling factors. *Geomorphology* 299: 142–151, DOI 10.1016/j.geomorph.2017.09.029.
- Huntley DJ, 2006. An explanation of the power-law decay of luminescence. *Journal of Physics: Condensed Matter* 18(4): 1359–1365, DOI 10.1088/0953-8984/18/4/020.
- Huntley DJ and Baril MR, 1997. The K content of the K-feldspars being measured in optical dating or in thermoluminescence dating. *Ancient TL* 15: 11–13.
- Huntley DJ and Lamothe M, 2001. Ubiquity of anomalous fading in K-feldspars and the measurement and correction for it in optical dating. *Canadian Journal of Earth Sciences* 38(7): 1093–1106, DOI 10.1139/cjes-38-7-1093.
- Kapp P, Pelletier JD, Rohrmann A, Heermance R, Russell J and Ding L, 2011. Wind erosion in the Qaidam basin, central Asia: Implications for tectonics, paleoclimate, and the source of the Loess Plateau. *Geological Society of America Today* 21(4–5): 4–10, DOI 10.1130/GSATG99A.1.
- Kars RH, Reimann T and Wallinga J, 2014. Are feldspar SAR protocols appropriate for post-IR IRSL dating? *Quaternary Geochronology* 22: 126–136, DOI 10.1016/j.quageo.2014.04.001.
- Kars RH, Wallinga J and Cohen KM, 2008. A new approach towards anomalous fading correction for feldspar IRSL dating – tests on samples in field saturation. *Radiation Measurements* 43(2–6): 786–790, DOI 10.1016/j.radmeas.2008.01.021.
- King GE, Christoph B, Roberts HM, and Pearceb NJG, 2018. Age determination using feldspar: Evaluating fading-correction model performance. *Radiation Measurements* 119: 58–73, DOI 10.1016/j.radmeas.2018.07.013.
- Kreutzer S, Burow C, Dietze M, Fuchs MC, Schmidt C, Fischer M and Friedrich J, 2019. Luminescence: Comprehensive Luminescence Dating Data Analysis. R package version 0.9.0.109. <https://CRAN.R-project.org/package=Luminescence>.
- Lai ZP, Mischke S and Madsen DB, 2014. Paleoenvironmental implications of new OSL dates on the formation of the “Shell Bar” in the Qaidam Basin, northeastern Qinghai-Tibetan Plateau. *Journal of Paleolimnology* 51: 197–210, DOI 10.1007/s10933-013-9710-1.
- Lai ZP and Ou XJ, 2013. Basic procedures of optically stimulated luminescence (OSL) dating. *Progress in Geography* 32(5): 683–693 (in Chinese with English abstract), DOI 10.11820/dlkxjz.2013.05.001.
- Li B and Li SH, 2011. Luminescence dating of K-feldspar from sediments: A protocol without anomalous fading correction. *Quaternary Geochronology* 6: 468–479, DOI 10.1016/j.quageo.2011.05.001.
- Li B and Li SH, 2012. A reply to the comments by Thomsen et al. on “Luminescence dating of K-feldspar from sediments: A protocol without anomalous fading correction”. *Quaternary Geochronology* 8: 49–51, DOI 10.1016/j.quageo.2011.10.001.
- Li GQ, Madsen DB, Jin M, Stevens T, Tao SX, She LL, Yang LP, Li FL, Wei HT, Duan YW and Chen FH, 2018. Orbital scale lake

- evolution in the Ejina Basin, central Gobi Desert, China revealed by K-feldspar luminescence dating of paleolake shoreline features. *Quaternary International* 482: 109–121, DOI 10.1016/j.quaint.2018.03.040.
- Li JY, Dong ZB, Qian, GQ, Zhang ZC, Luo WY, Lu JF, Wang M, 2016. Yardangs in the Qaidam Basin, northwestern China: Distribution and morphology. *Aeolian Research* 20: 89–99, DOI 10.1016/j.aeolia.2015.11.002.
- Liu JF, Murray AS, Buylaert JP, Jain M, Chen J and Lu YC, 2016. Stability of fine-grained TT-OSL and post-IR IRSL signals from a c. 1 Ma sequence of aeolian and lacustrine deposits from the Nihevan Basin (northern China). *Boreas* 45(4): 703–714, DOI 10.1111/bor.12180.
- Mischke S, Madsen D, Zhang CJ and Lai ZP, 2015. Reply to comment by Zhang (2014): The Shell Bar in the Qaidam Basin: fluvial or lake deposit, and OSL versus 14 C age data. *Journal of Paleolimnology* 53: 335–344, DOI 10.1007/s10933-014-9817-z.
- Murray AS and Wintle AG, 2000. Luminescence dating of quartz using an improved single aliquot regenerative-dose protocol. *Radiation Measurements* 32: 57–73, DOI 10.1016/S1350-4487(99)00253-x.
- Murray AS and Wintle AG, 2003. The single aliquot regenerative dose protocol: potential for improvements in reliability. *Radiation Measurements* 37: 377–381, DOI 10.1016/S1350-4487(03)00053-2.
- Pullen A, Kapp P, McCallister AT, Chang H, Gehrels G E, Garzzone CN, Heermance RV and Ding L, 2011. Qaidam Basin and northern Tibetan Plateau as dust sources for the Chinese Loess Plateau and paleoclimatic implications. *Geology* 39(11): 1031–1034, DOI 10.1130/G32296.1.
- Qin JT and Zhou LP, 2012. Effects of thermally transferred signals in the post-IR IRSL SAR protocol. *Radiation Measurements* 47: 710–715, DOI 10.1016/j.radmess.2011.12.011.
- Rees-Jones J, 1995. Optical dating of young sediments using fine-grained quartz. *Ancient TL* 13: 9–14.
- Roberts HM, 2012. Testing Post-IR IRSL protocols for minimising fading in feldspars, using Alaskan loess with independent chronological control. *Radiation Measurements* 47(9): 716–724, DOI 10.1016/j.radmeas.2012.03.022.
- Roberts HM and Duller GAT, 2004. Standardised growth curves for optical dating of sediment using multiple-grain aliquots. *Radiation Measurements* 38: 241–252, DOI 10.1016/j.radmeas.2003.10.001.
- Rohrmann A, Heermance R, Kapp P and Cai FL, 2013. Wind as the primary driver of erosion in the Qaidam Basin, China. *Earth and Planetary Science Letters* 374: 1–10, DOI 10.1016/j.epsl.2013.03.011.
- Spratt RM and Lisiecki LE, 2016. A Late Pleistocene sea level stack. *Climate of the Past* 12: 1079–1092, DOI 10.5194/cp-12-1079-2016.
- Sun YJ, Lai ZP, Long H, Liu XJ and Fan QS, 2010. Quartz OSL dating of archaeological sites in Xiao Qaidam Lake of the NE Qinghai-Tibetan Plateau and its implications for palaeoenvironmental changes. *Quaternary Geochronology* 5(2): 360–364, DOI 10.1016/j.quageo.2009.02.013.
- Thiel C, Buylaert JP, Murray AS and Tsukamoto S, 2011. On the applicability of post-IR IRSL dating to Japanese loess. *Geochronometria* 38(4): 369–378, DOI 10.2478/s13386-011-0043-4.
- Thomsen KJ, Murray AS and Jain M, 2011. Stability of IRSL signals from sedimentary K-feldspar samples. *Geochronometria* 38(1): 1–13, DOI 10.2478/s13386-011-0003-z.
- Thomsen KJ, Murray AS, Jain M and Bøtter-Jensen L, 2008. Laboratory fading rates of various luminescence signals from feldspar-rich sediment extracts. *Radiation Measurements* 43(9): 1474–1486, DOI 10.1016/j.radmeas.2008.06.002.
- Wang J, Xiao L, Reiss D, Hiesinger H, Huang J, Xu Y, Zhao JN, Xiao ZY and Komatsu G, 2018. Geological Features and Evolution of Yardangs in the Qaidam Basin, Tibetan Plateau (NW China): A Terrestrial Analogue for Mars. *Journal of Geophysical Research: Planets* 123: 2336–2364, DOI 10.1029/2018JE005719.
- Wu L, Prush V, Lin X, Xiao A, Zhang L, Chen N, Yang R and Chen H, 2019. Quantifying wind erosion during the late Quaternary in the Qaidam Basin, Central Asia. *Geophysical Research Letters* 46(12): 6378–6387, DOI 10.1029/2019GL082992.
- Xiao L, Wang J, Dang YN, Cheng ZY, Huang T, Zhao JN, Xu Y, Huang J, Xiao ZY and Komatsu G, 2017. A new terrestrial analogue site for Mars research: The Qaidam Basin, Tibetan Plateau (NW China). *Earth-Science Reviews* 164: 84–101, DOI 10.1016/j.earscirev.2016.11.003.
- Yu LP, An P and Lai ZP, 2016. Different Implications of OSL and radiocarbon ages in archaeological sites in the Qaidam Basin, Qinghai-Tibet Plateau. *Geochronometria* (43): 188–200, DOI 10.1515/geochr-2015-0048.
- Yu LP, Dong ZB, Lai ZP, Qian GQ and Pan T, 2015a. Origin and lateral migration of linear dunes in the Qaidam Basin of NW China revealed by dune sediments, internal structures, and optically stimulated luminescence ages, with implications for linear dunes on Titan: Comment and Discussion. *Geological Society of America Bulletin* 127 (1–2): 316–320, DOI 10.1130/B31041.1.
- Yu LP and Lai ZP, 2012. OSL chronology and palaeoclimatic implications of aeolian sediments in the eastern Qaidam Basin of the northeastern Qinghai-Tibetan Plateau. *Palaeogeography, Palaeoclimatology, Palaeoecology* 337–338: 120–129, DOI 10.1016/j.palaeo.2012.04.004.
- Yu LP and Lai ZP, 2014. Holocene climate change inferred from stratigraphy and OSL chronology of aeolian sediments in the Qaidam Basin, northeastern Qinghai-Tibetan Plateau. *Quaternary Research* 81(3): 488–499, DOI 10.1016/j.yqres.2013.09.006.
- Yu LP, Lai ZP and An P, 2013. OSL chronology and paleoclimatic implications of paleodunes in the middle and southwestern Qaidam Basin, Qinghai-Tibetan Plateau. *Sciences in Cold and Arid Regions* 5(2): 211–219, DOI 10.3724/SP.J.1226.2013.00211.
- Yu LP, Lai ZP, An P, Pan T and Chang QF, 2015b. Aeolian sediments evolution controlled by fluvial processes, climate change and human activities since LGM in the Qaidam Basin, Qinghai-Tibetan Plateau. *Quaternary International* 372: 23–32, DOI 10.1016/j.quaint.2014.09.043.
- Yu LP, Roskin J and Greenbaum N, 2019. Aeolian-Fluvial Interactions Stabilize Desert in the Qaidam Basin, Qinghai-Tibetan Plateau. *Geophysical Research Abstracts* 21, EGU2019-19084.
- Yu SS, Tan HB, Liu XQ, Cao GC, 2009. Study on Sustainable Utilization of Resources in Qarhan Salt Lake. Science Press: Beijing (in Chinese).
- Yu SY, Colman SM and Lai ZP, 2018. Late-Quaternary history of ‘great lakes’ on the Tibetan Plateau and palaeoclimatic implications – A review. *Boreas* 48(1): 1–19, DOI 10.1111/bor.12349.
- Zhang HC, Fan HF, Chang FQ, Zhang WX, Lei GL, Yang MS, Lei YB and Yang LQ, 2008. AMS Dating on the Shell Bar Section from Qaidam Basin, NE Tibetan Plateau, China. *Radiocarbon* 50(2): 255–265, DOI 10.1017/S0033822200033555.
- Zheng D and Zhao D, 2017. Characteristics of natural environment of the Tibetan Plateau. *Science & Technology Review* 35(6): 13–22 (in Chinese with English abstract).
- Zhang ZF, Zhang HP and Ma XP, 2014. Change features of average wind speed and strong wind days in Chaidamu Basin. *Journal of Arid Land Resources and Environment* 28(10): 90–94, DOI 10.13448/j.cnki.jalre.2014.10.015 (in Chinese with English abstract).